Electronic Supplementary Material (ESI) for ChemComm.

Supporting Information

Tailoring Fluorescent ZIF-8 Nanostructures through Calix[4]pyrrole Modification: Tunable Size and Enhanced Organic Micropollutant Removal Capacity

Contents: **Page**

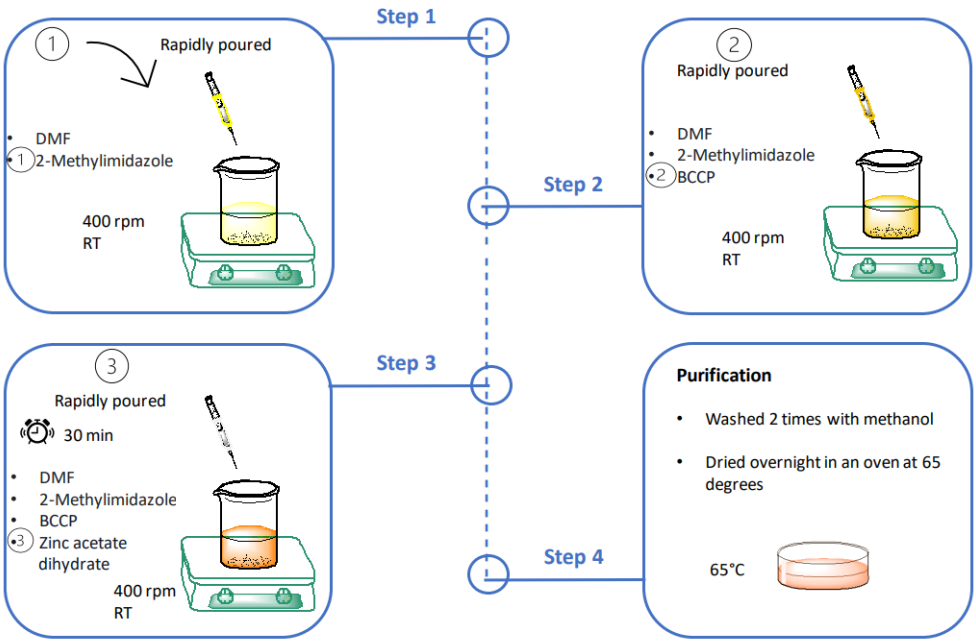

Scheme S1. Schematic illustration of synthesis of BCCP modified ZIF-8 structures

Materials & Methods

The bis-carboxylate functional calix[4]pyrrole (BCCP) was synthesized according to the literature [1].

Synthesis of bis-carboxylate functional calix[4]pyrrole modified ZIF-8 structures

In the main reaction beaker, 0.6568 g of 2-methylimidazole (mIM, 8 mmol) was dissolved in 20 mL of DMF. The other main solution consisted of 0.2194 g of zinc acetate dihydrate (Zn(OAc), 1 mmol) dissolved in 10 mL of DMF. Additionally, BCCP solutions were prepared with different concentrations by using following amounts: 0.1 mmol (I) and 0.01 mmol (II), each dissolved in 10 mL of DMF. The mIM solution was mixed at 400 rpm, and then the bis-carboxylate functional calix[4]pyrrole solution was rapidly added into the mIM solution. Subsequently, the Zn^{2+} solution was quickly poured into the reaction medium. After stirring at room temperature for 30 minutes, ZIF-8 nanocrystals were synthesized. The nanocrystals were then washed twice with fresh methanol and dried overnight in an oven at 65°C.

Structural and Optical Characterization

After synthesizing and purifying the product, the emission color of bis-carboxylate functional calix[4]pyrrole and bis-carboxylate functional calix[4]pyrrole modified ZIF-8 structures were observed under a UV lamp with an illumination wavelength of 366 nm. To characterize the optical properties, bis-carboxylate functional calix[4]pyrrole and each bis-carboxylate

functional calix[4]pyrrole modified ZIF-8 structures were dissolved in DMF and the absorption spectrum was recorded using a Varian Cary double-beam ultraviolet-visible (UV-vis) spectrophotometer. Additionally, a Varian Cary Eclipse Fluorescence Spectrofluorometer was used to record the excitation and emission spectra of each sample in order to understand their emission properties. To avoid self-absorption, the optical density of each sample type was adjusted to 0.1 at 350 nm before collecting the emission and excitation spectra. The emission spectrum was collected at 3 different excitation wavelengths; 300 nm, 350 nm and 400 nm. The excitation spectrum was collected at 3 different emission wavelengths; 365 nm, 400 nm, 500 nm. The quantum yield of each carbon dot was calculated using Coumarin 102 as a reference, following the methodology described in the literature [2]. All the measurements were done at room temperature.

For the structural characterization of bis-carboxylate functional calix[4]pyrrole and bis-carboxylate functional calix[4]pyrrole modified ZIF-8 structures, X-Ray diffraction (XRD) , Raman microspectroscopy, Fourier transform infrared spectroscopy (FTIR) measurements were conducted.

The crystal structure of ZIF-8 and bis-carboxylate functional calix[4]pyrrole modified ZIF-8 structures were analyzed using a RIGAKU SmartLab X-ray diffraction spectrometer with Cu Kα radiation at a wavelength of 1.5406 Å and a voltage of 45 kV. The XRD measurements were performed in the 2-theta range from 5° to 40° with a 4-second speed for each data point, using a step size of 0.01 degrees. The surface characteristics of the ZIF-8, bis-carboxylate functional calix[4]pyrrole and bis-carboxylate functional calix[4]pyrrole modified ZIF-8 structures were analyzed using a PerkinElmer ATR-FTIR spectrophotometer. Raman spectrum of ZIF-8 and bis-carboxylate functional calix[4]pyrrole were collected using a RENISHAW inVia spectrometer with 532 nm excitation laser, 0.01% laser power, 10 s acquisition time, and x50 objective lens at room temperature.

Micropollutant Removal Experiments

The assessment of micropollutants adsorbed from water involved quantifying the remaining micropollutant amounts through UV/Vis spectroscopy. Calibration curves were established autonomously, employing standardized micropollutant solutions in water.

The procedure for micropollutant removal was conducted as follows: Independently, 1 mL of a micropollutant solution (25.5 μM) was shaken with a 5 mg sample for 2 hours using a 400 rpm shaker, and the mixture was enclosed with aluminum foil. Following phase separation, a 0.3

mL portion of the samples was diluted to 3 mL with water and analyzed using UV/Vis spectrometry.

The positions of XRD Peaks:

The position of the prominent XRD peaks was attributed to the following planes: 7.34, 10.35, 12.75, 14.74, 16.50, 18.02, 19.49, 22.16, 24.56, 25.64, 26.71, 29.67, 30.65, 31.48, 32.51, 35.01, 36.48 which corresponds to plane (110), (200), (211), (220), (310), (222), (321), (411), (332), (422), (431), (440), (433), (442), (611), (622), (444), respectively (Fig.1).

TEM images of ZIF-8 BCCP(I)

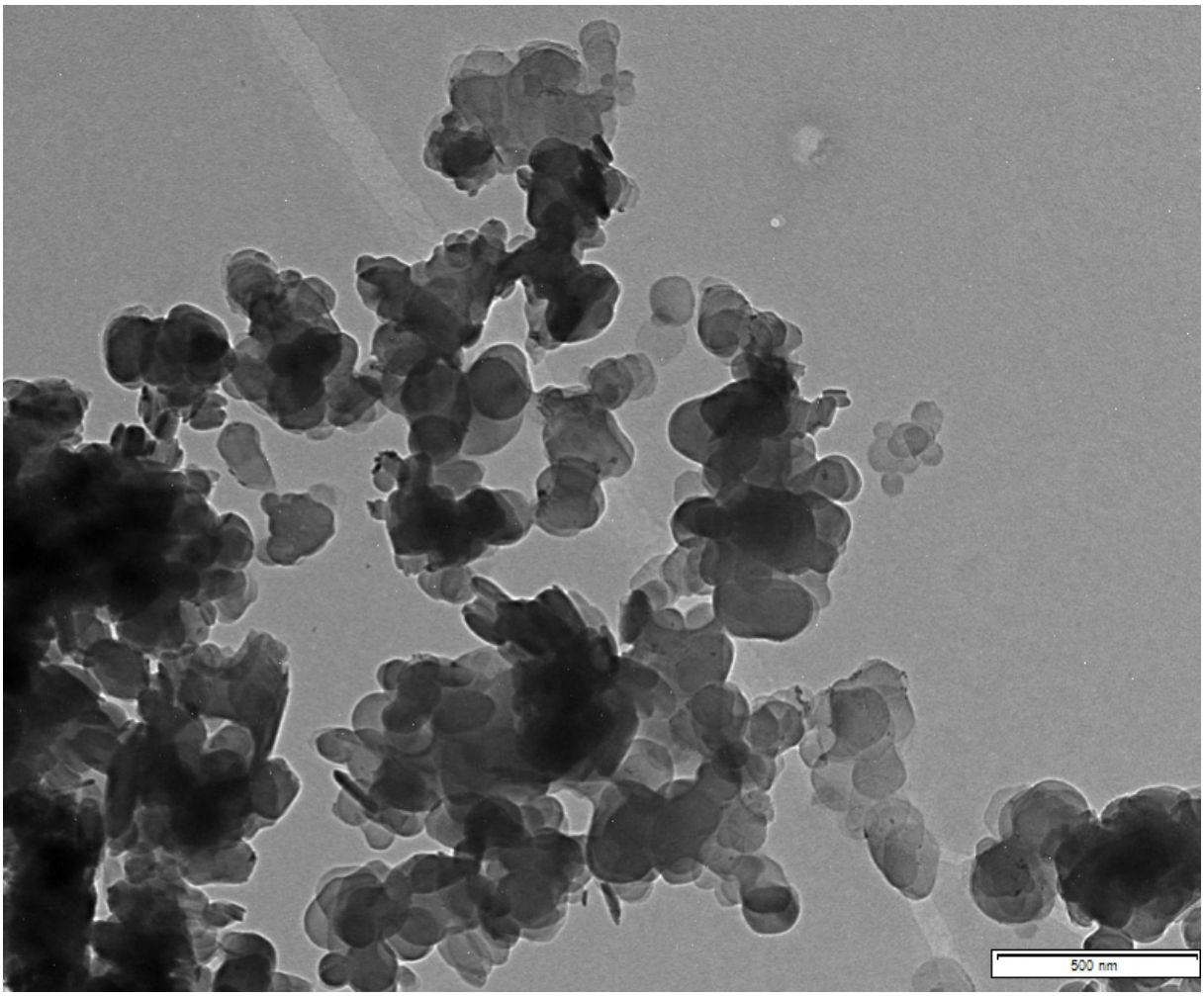

Fig. S1 TEM images of ZIF-8 BCCP(I).

Brunauer–Emmett–Teller (BET) analysis of modified and non-modified ZIF-8

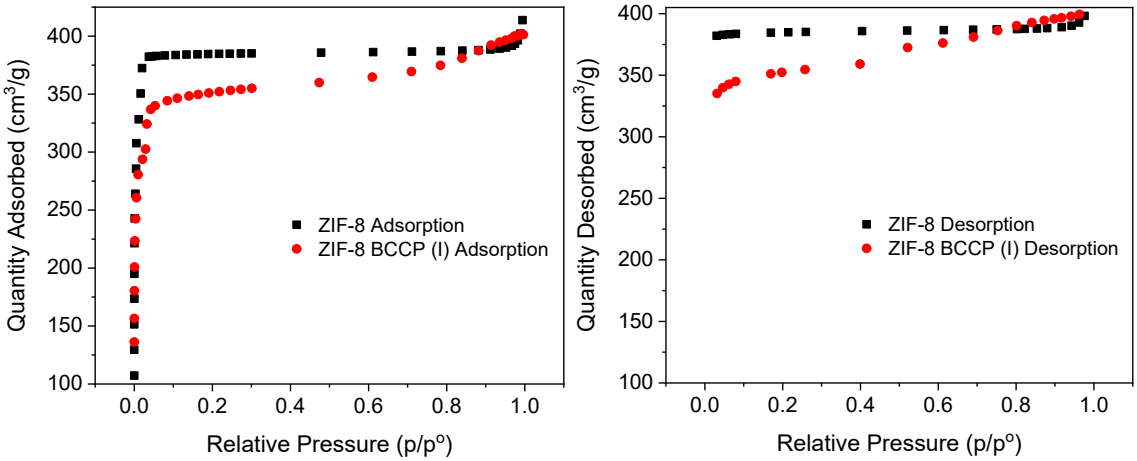

Fig. S2 Nitrogen sorption isotherms (adsorption on the left, desorption on the right) of ZIF-8 and ZIF-8 BCCP (I)

Table S2. Surface areas, pore volumes and pore sizes of prepared ZIF-8 structures

Surface Area (m^2/g)	**ZIF-8**	**ZIF-8 BCCP (I)**
BET Surface Area	1146.5941	1059.8276
Adsorption cumulative surface area of pores	5.311	46.384
Desorption cumulative surface area of pores	10.0116	89.5632
Pore Volume (cm^3/g)	**ZIF-8**	**ZIF-8 BCCP (I)**
Micropore volume	0.586426	0.492091
Adsorption cumulative volume of pores	0.046759	0.097112
Desorption cumulative volume of pores	0.048890	0.115429
Pore Size (Å)	**ZIF-8**	**ZIF-8 BCCP (I)**
Adsorption average pore width	352.147	83.746
Desorption average pore width	195.334	51.552

FTIR and Raman spectra of ZIF-8, modified ZIF-8 and BCCP

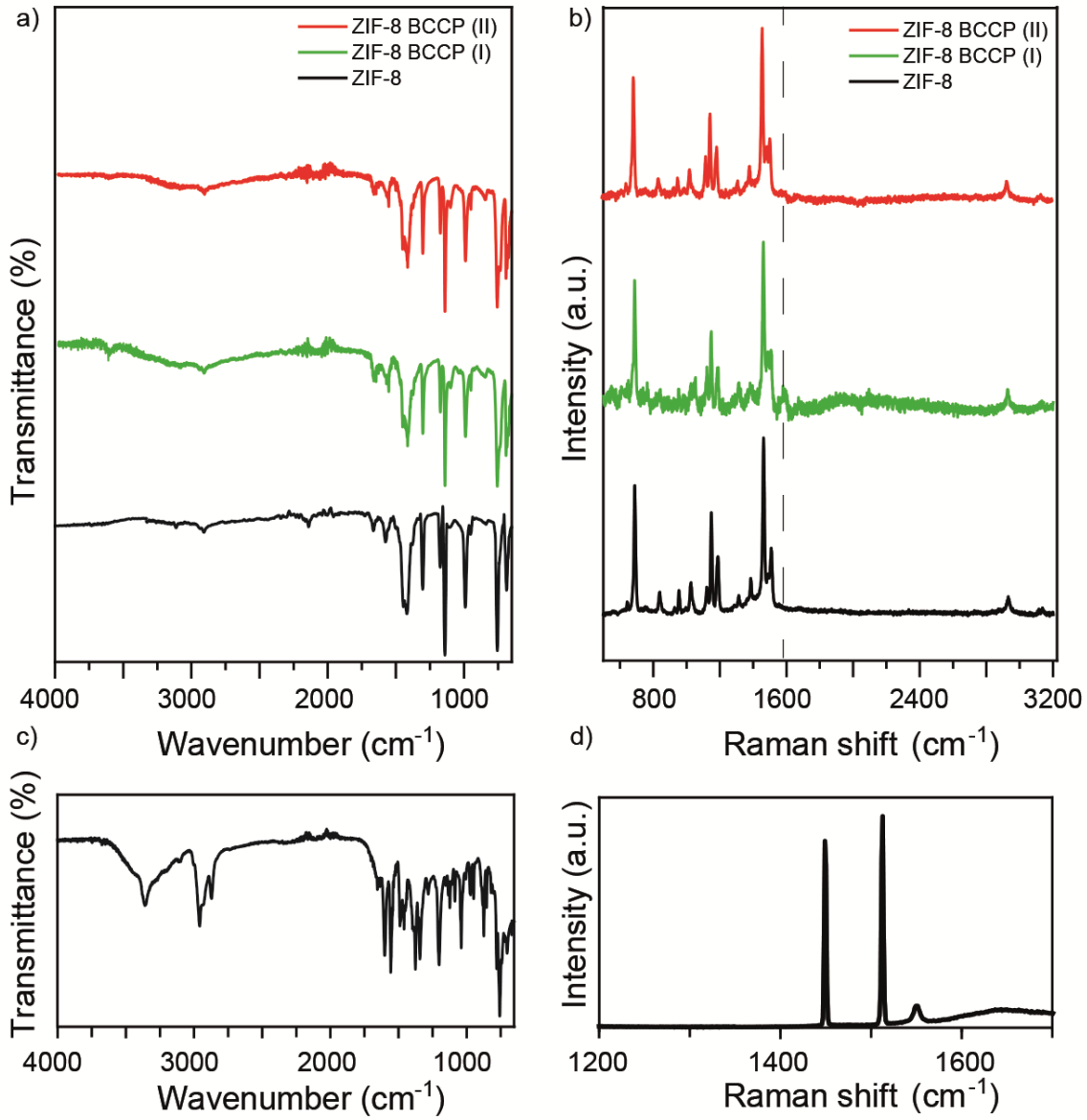

Fig. S3 a) FTIR and **b**) Raman spectra of non-modified ZIF-8 and BCCP modified ZIF-8 structures. The gray dashed line in the Raman spectra corresponds to 1560 cm^{-1}. **c)** FTIR spectrum of BCCP **d)** Raman spectrum of BCCP. Two intense peaks around 1440 cm^{-1} and 1510 cm^{-1} were attributed to sp^2 hybridized carbon atoms in the calix[4]pyrrole. The peak at 1560 cm^{-1} was attributed to the presence of pyrrole units.[4]

Photoluminescence Excitation (PLE) Spectrum of modified and non-modified ZIF-8

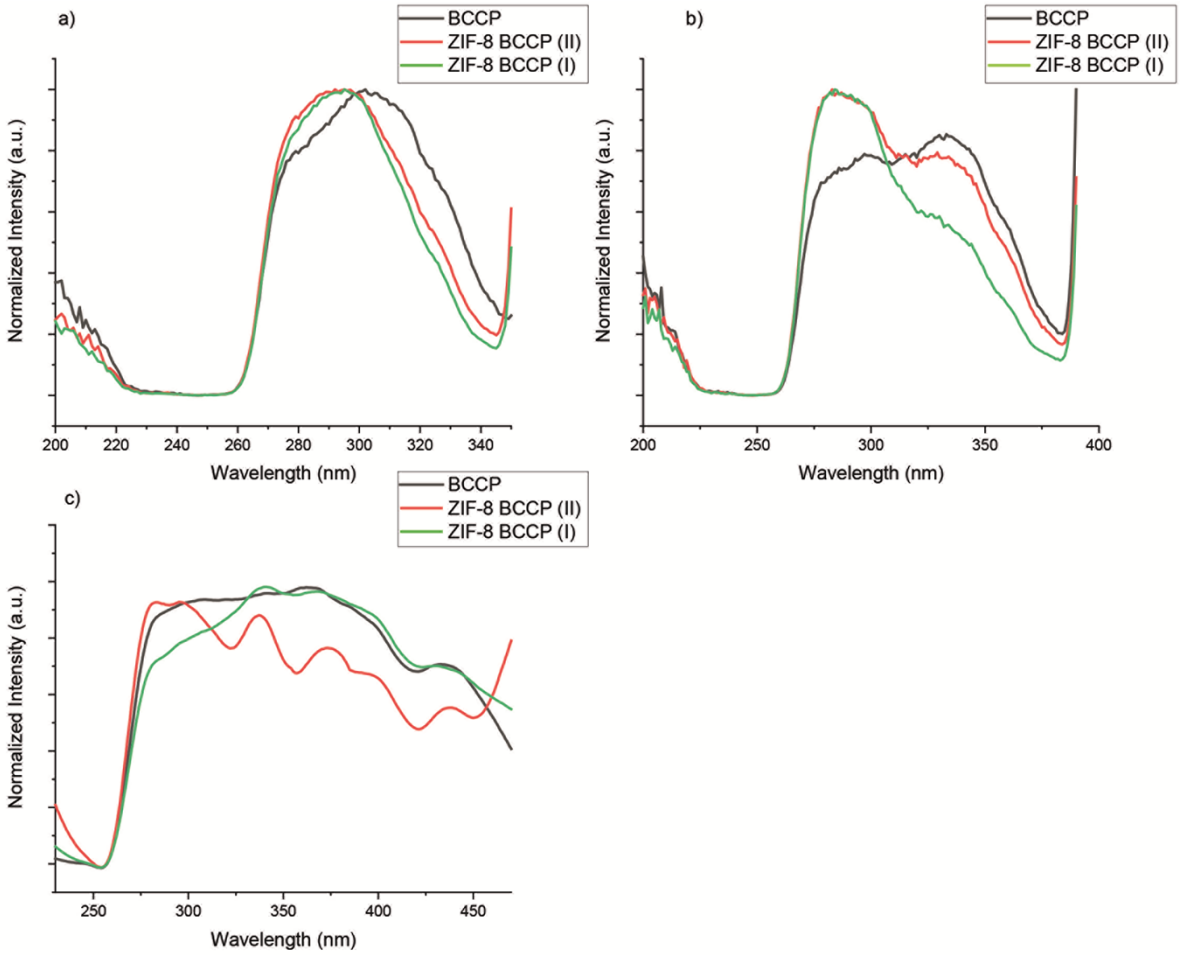

Fig. S4 Excitation spectra of non-modified ZIF-8 and BCCP modified ZIF-8 at different emission wavelengths; a) 365 nm, b) 400 nm, c) 500 nm.

To shed light on the differences in radiative transitions between BCCP and BCCP-modified ZIF-8, photoluminescence excitation (PLE) spectra were collected for each material at three distinct emission wavelengths (365, 400, and 500 nm) (Fig. S4). The PLE spectra of both BCCP and BCCP-modified ZIF-8 were similar at an emission wavelength of 366 nm, exhibiting a single peak around 295 nm (Fig. S4). However, in ZIF-8 BCCP(I), where the BCCP concentration was highest, the peak showed a slight broadening. On the other hand, the PLE spectrum of BCCP and the PLE spectra of BCCP-modified ZIF-8 differed significantly at 400 nm (Fig. S4). At this emission wavelength, the PLE spectrum of BCCP displayed two major peaks: one at 295 nm and another at 335 nm. Notably, the peak at 295 nm was twice as intense as the peak at 335 nm in BCCP. However, as BCCP integrated into the ZIF-8 structure, the ratio between intensities of the peaks at 295 and 335 nm changed dramatically. As the BCCP concentration increased, the relative ratio of the peak at 335 nm increased and for ZIF-8

BCCP(I), the intensity of the peak at 335 nm was higher by 15% than the intensity of the peak at 295 nm. These results concluded that as the BCCP amount in ZIF-8 increased, the radiative decay at 400 nm could be excited more by 335 nm excitation. Additionally, the excitation spectra at 500 nm emission are given in Fig. 4c and exhibited significant differences when comparing the excitation spectrum of BCCP and the excitation spectra of BCCP-modified ZIF-8. PLE spectrum of BCCP showed a broad peak covering the range from 260 nm to 460 nm, with a slight decrease in intensity within the 360 – 460 nm range. Conversely, the BCCP-modified ZIF structures also displayed a similar peak in the PLE spectrum, but with slightly lower intensity within the 275 – 325 nm range. As the amount of BCCP increased, the intensity of this peak decreased further within the aforementioned range. It is worth noting that the PLE spectrum of ZIF-8 with the lowest amount of BCCP (ZIF-8 BCCP (II)) exhibited entirely different characteristics. In this case, the peak had its maximum at 300 nm, and the intensity gradually decreased until 450 nm. These results show that the fluorescence induction of BCCP at 500 nm underwent alterations as BCCP surrounded the ZIF-8 crystals, leading to a whiter fluorescence.

Solubility of BCCP and BCCP modified ZIF-8 in water

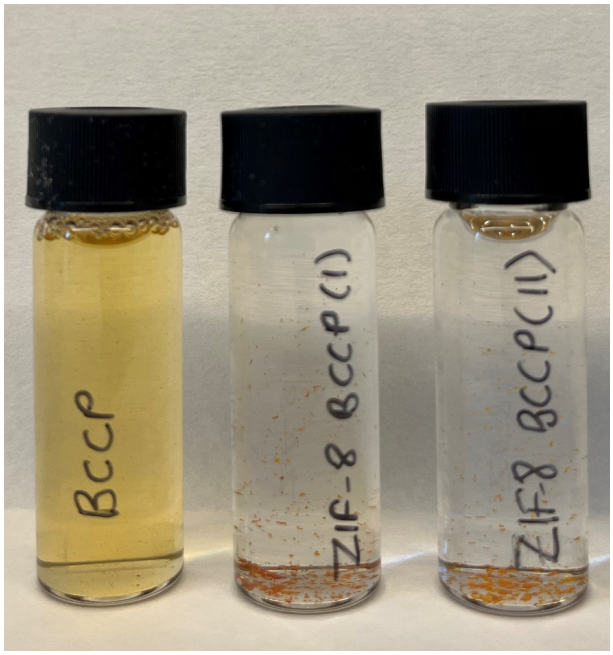

Fig. S5 Solubility of BCCP and BCCP modified ZIF-8 structures in pure water. The BCCP molecule was soluble in water, however, the ZIF-8 BCCP(I) and ZIF-8 BCCP(II) were not soluble in water.

Calculation of Removal efficiencies and Calibration Curves of Dyes

The removal efficiency (R) of each ZIF-8 for each dye was calculated by using the following equation;

$$R = \frac{c_0 - c_e}{c_0} \times 100\%$$

Where c_0 (μM) is the initial dye concentration and c_e (μM) is the dye concentration after ZIF-8 treatment. The calibration curves for each dye indicated that the concentration of 25.5 μM for each dye remained within the linear region for absorption values, allowing the application of Beer's Law.

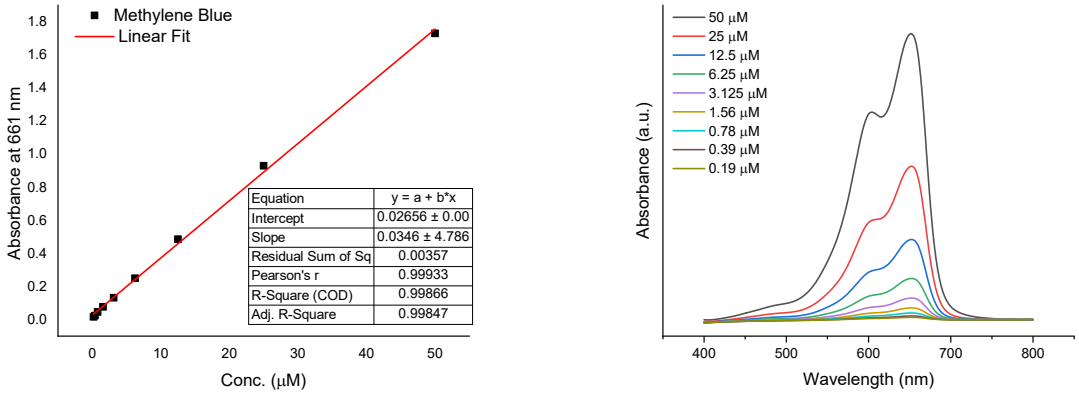

Fig. S6 Calibration curve generated by measuring the absorbance values at 661 nm produced by standardized solutions of methylene blue (left) and UV/Vis spectra (right) of standardized methylene blue solutions.

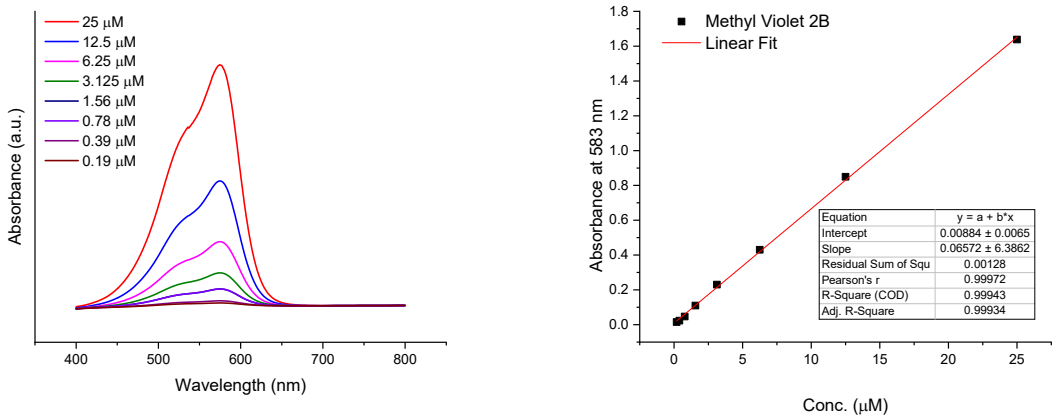

Figure S7. Calibration curve generated by measuring the absorbance values at 583 nm produced by standardized solutions of methyl violet (left) and UV/Vis spectra (right) of standardized methyl violet solutions.

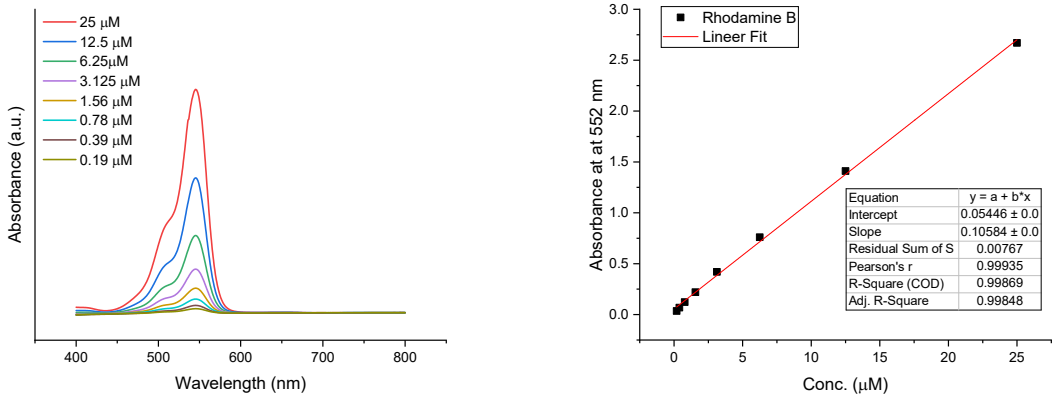

Figure S8. Calibration curve generated by measuring the absorbance values at 552 nm produced by standardized solutions of rhodamine B (left) and UV/Vis spectra (right) of standardized rhodamine B solutions.

^{1}H-NMR SPECTRUM OF BIS-CARBOXYLATE FUNCTIONAL CALIX[4]PYRROLE

^{1}H NMR (500 MHz, CD_3CN) δ 9.79 (s, 4H), 5.81 (t, *J* = 3.2 Hz, 4H), 5.75 (dd, *J* = 2.6 Hz, 4H), 3.16-3.12 (m, *J* = 8.3 Hz, 16H), 1.68 (s, 6H, CH2), 1.65 – 1.60 (m, 16H,CH2), 1.45 (s, 12H,CH3), 1.38 (d, *J* = 7.5 Hz, 16H,CH2), 1.01 (d, *J* = 7.4 Hz, 24H,CH).

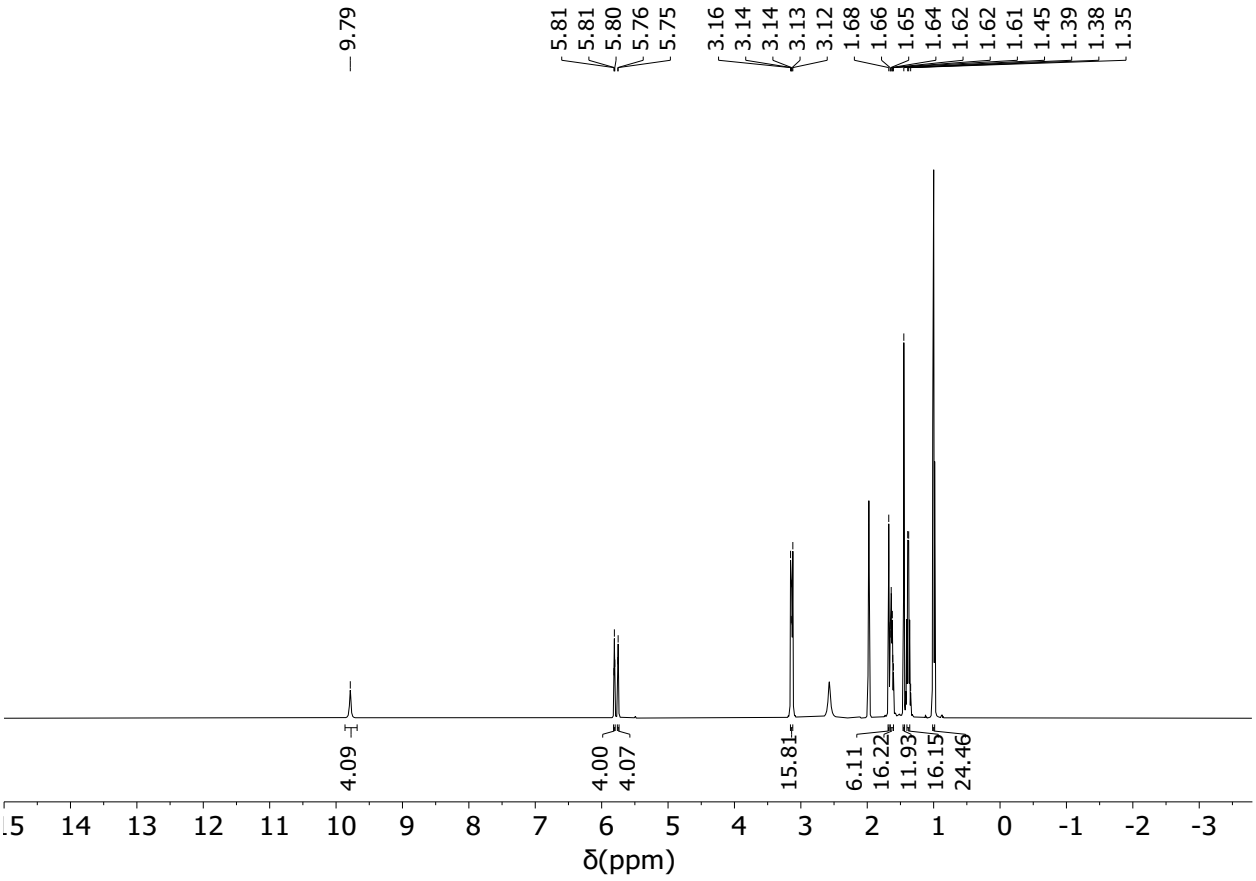

Figure S9. ^{1}H NMR spectrum of the compound recorded in CD_3CN.

^{13}C-NMR SPECTRUM OF BIS-CARBOXYLATE FUNCTIONAL CALIX[4]PYRROLE

^{13}C NMR (126 MHz, CD_3CN) δ 177.10, 137.71, 136.78, 102.16, 101.05, 58.75, 46.93, 35.24, 30.31, 24.09, 23.45, 19.68, 13.70.

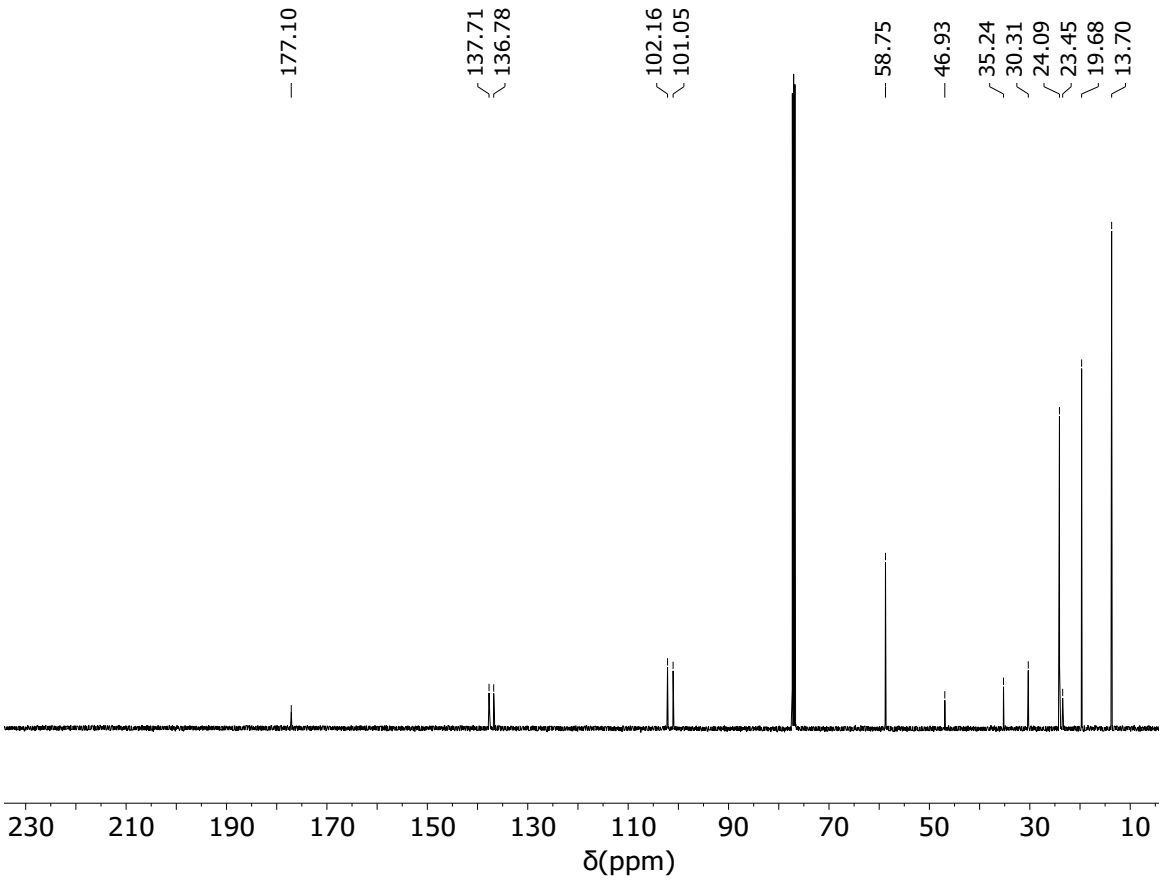

Figure S10. ^{13}C NMR spectrum of the compound recorded in CD_3CN.

REFERENCES

1 F. Yelda Ünlü and A. Aydogan, *Macromol. Rapid Commun.*, 2022, **43**, 2200447.

2 C. Ünlü, *Opt. Mater. (Amst).*, 2019, **89**, 361–367.

3 B. Tang, Y. Dai, Y. Sun, H. Chen and Z. Wang, *J. Solid State Chem.*, 2020, **284**, 121215.

4 Y. Su, H. Zhu and H. Dong, Anal. Lett., 2015, 48, 477-488.